



## Research article

# Thermohydraulic performance investigation of a heat exchanger with combined effect of ribbed insert and Therminol55/MXene+Al<sub>2</sub>O<sub>3</sub> nanofluid: A numerical two-phase approach

Likhan Das<sup>a,\*\*</sup>, Navid Aslfattahi<sup>b,\*\*\*</sup>, Khairul Habib<sup>c</sup>, R. Saidur<sup>d,e</sup>, Anupom Das<sup>f</sup>, Kumaran Kadirgama<sup>g,h,\*</sup><sup>a</sup> Department of Industrial and Manufacturing Systems Engineering, Iowa State University, 515 Morrill Road, Iowa, Ames, 50011, USA<sup>b</sup> Department of Fluid Mechanics and Thermodynamics, Faculty of Mechanical Engineering, Czech Technical University in Prague, Technická 4, 166 07 Prague, Czech Republic<sup>c</sup> Department of Mechanical Engineering, Universiti Teknologi PETRONAS, Perak, 32610, Malaysia<sup>d</sup> Research Centre for Nanomaterials and Energy Technology (RCNMET), School of Engineering and Technology, Sunway University, 47500, Petaling Jaya, Malaysia<sup>e</sup> Department of Engineering, Lancaster University, Lancaster, LA1 4YW, UK<sup>f</sup> Department of Urban and Regional Planning, Chittagong University of Engineering and Technology, Chittagong, Bangladesh<sup>g</sup> Faculty of Mechanical and Automotive Engineering Technology, Universiti Malaysia Pahang, Pekan 26600, Malaysia<sup>h</sup> Advanced Nano Coolant-Lubricant (ANCL) Lab, Automotive Engineering Centre, Universiti Malaysia Pahang, Pekan, 26600, Malaysia

## ARTICLE INFO

## Keywords:

MXene  
Nanofluid  
Heat exchanger  
Insert turbulator

## ABSTRACT

MXene-based nanofluids are novel trends with improved dispersion stability and thermophysical characteristics over previously established nanofluids. In the present work, the thermohydraulic characteristics of a double pipe heat exchanger (DPHEX) with a Therminol55 (TH55)/MXene + Al<sub>2</sub>O<sub>3</sub> nanofluid and various geometrically shaped (triangular, rectangular) ribbed twisted tape (TT) inserts are numerically investigated using the ANSYS Fluent interface. A counter flow arrangement with three different types of inserts (RRTT, TRTT, TT) and TH55/MXene + Al<sub>2</sub>O<sub>3</sub> nanofluid at 0.20 wt% are studied inside the heat exchanger. Adding ribbed inserts to the conventional TT insert enhances the turbulence intensity by creating extra vortices. The thermal boundary layer grows thinner due to increased axial and radial velocity. Due to the substantial flow obstruction, adding ribs increases the overall pressure drop between the inlet and outlet. The maximum increase in *Nu* is 11.04 % using nanofluid instead of water, whereas the combination of insert and nanofluid exhibited up to 105 % enhancement for rectangular-ribbed TT compared to the plain tube. Nevertheless, the pressure decrease is found to be maximum in rectangular-ribbed TT because of significant flow disruption. This was likewise true with triangular-ribbed TT and TT insert. According to the PEC assessment, the RRTT insert had a maximum PEC value of 1.67 greater than TRTT and traditional TT for both TH55 and nanofluid flowing inside the tube. To summarize, the combination of TH55/MXene + Al<sub>2</sub>O<sub>3</sub> RRTT insert may be a promising choice for improving heat exchanger performance in a new generation efficient thermal system.

\* Corresponding author.

\*\* Corresponding author.

\*\*\* Corresponding author.

E-mail addresses: [likhan.das11@gmail.com](mailto:likhan.das11@gmail.com) (L. Das), [navid.fth87@yahoo.com](mailto:navid.fth87@yahoo.com) (N. Aslfattahi), [kumaran@ump.edu.my](mailto:kumaran@ump.edu.my) (K. Kadirgama).<https://doi.org/10.1016/j.heliyon.2023.e14283>

Received 22 November 2022; Received in revised form 20 February 2023; Accepted 28 February 2023

Available online 9 March 2023

2405-8440/© 2023 The Authors. Published by Elsevier Ltd. This is an open access article under the CC BY-NC-ND license (<http://creativecommons.org/licenses/by-nc-nd/4.0/>).

## 1. Introduction

Researchers are stepping up their efforts to increase heat transfer performance by employing a variety of active and passive strategies in attempt to develop highly efficient and compressed thermal energy systems. The rate of heat exchange inside the heat exchanger has a major effect on the overall performance of thermal systems such as absorption chillers [1], thermoelectric generators [2], air conditioning [3], and photovoltaic cooling [4]. Passive heat transfer enhancement techniques are more favorable than active heat transfer enhancement techniques since they do not require an external power source. Since the term 'nanofluid' was coined by [5] in 1995, nanofluid has revolutionized heat transfer enhancement. The tremendous popularity and research interest in nanofluids over the past two decades has spurred researchers to develop novel nanofluids in addition to tackling existing challenges such as stability and cost reduction in the process of formulating sustainable nanofluids.

Significant improvement in heat transfer performance can be perceived by incorporating nanofluids instead of conventional heat transfer fluid owing to their higher thermal conductivity as compared to the base fluids [6, 7]. For example, Albadr, Tayal [8] experimentally investigated the heat transfer performance of a shell and tube heat exchanger with water/ $\text{Al}_2\text{O}_3$  nanofluid for different concentrations ranging between 0.3–2.0 vol%. A maximum 57% enhancement of overall heat transfer coefficient was reported for concentration 0.2 vol% of nanofluid with a 62.6% increase in Nusselt number than distilled water [9]. investigated a finned shell and tube heat exchanger and tested various volume concentrations of nanofluid to determine how they affected heat transmission. In the heat exchanger,  $\text{Fe}_2\text{O}_3$ /water nanofluids with volume concentrations of 1%, 1.5%, and 2% were used as heat transfer fluids, and the results were compared to pure water. It was discovered that utilizing nanofluid  $\text{Fe}_2\text{O}_3$ /water with a volume fraction of 2% can yield the maximum heat transfer rate enhancement of 19.1%. In another study by Afshari and Muratçobanoğlu [10], it was found that the thermal performance of a block heat sink significantly increased using  $\text{Fe}_2\text{O}_3$ /water based nanofluid at a concentration as low as 0.2 vol%. Singh and Sarkar [11] examined the impact of tapering coils in twin pipes on the thermo-physical properties of 50 nm  $\text{Al}_2\text{O}_3$  and 90 nm MgO with water as a base fluid at nanofluids inlet temperature (50 °C, 60 °C and 70 °C). For convergence, divergence, and convergence-divergence, the researchers used aluminum wire coils with a permanent 10 mm pitch. As Re grew, Nu and the friction factor declined, reducing momentum and thermal boundary layer thickness. Friction increased long-path flow. Strong contact between nanofluids and tube wall increased heat transfer in the divergence-style wire coil. In another study, Singh and Sarkar [11] examined the heat transfer and pressure drop of an  $\text{Al}_2\text{O}_3 + \text{TiO}_2$  nanofluid in a heat exchanger fitted with several modified V-cut twisted tape inserts. They took into account different twist ratios, V-cut depth/width ratios, and nanofluid temperatures. According to their findings, raising the depth ratio, decreasing the width ratio, and lowering the temperature of the nanofluid all increased heat transfer and pressure losses. The heat transfer rate and friction factor rose by 132% and 55%, respectively, in comparison to water in a plain tube. Fares, Al-Mayyahi [12] demonstrated 24.4% and 7.3 % enhancements in thermal efficiency on the hot and cold sides of a shell and tube heat exchanger, respectively, as well as a 13.7 % increase in mean thermal efficiency when using 0.2 wt % graphene/water nanofluids as the hot fluid on the tube side. Carbon nanotubes (SWCNT, MWCNT) and two-dimensional nanomaterials (Graphene, MXene) have gained enormous popularity in recent years due to their superior thermal conductivity, high specific surface area, and morphology, which allow them to produce nanofluids with better thermophysical properties than conventional metal and metal oxide-based nanofluids. In a comparative research, MWCNT/and graphene-based water nanofluids outperformed  $\text{TiO}_2$ ,  $\text{Al}_2\text{O}_3$ , ZnO,  $\text{CeO}_2$ , and hybrid ( $\text{Cu} + \text{Al}_2\text{O}_3$ ) based nanofluids in a plate heat exchanger [13]. Numerous studies have demonstrated the superiority of MXene, carbon nanotubes, and graphene in terms of heat transport qualities. Aslfattahi, Samyilingam [14] demonstrated a 64 % increase in thermal conductivity when 0.1 wt. % MXene was added to silicone oil. Another study conducted by Das, Habib [15] revealed a maximum improvement of 47% in thermal conductivity as a result of the introduction of MXene at a 0.2 wt.% loading concentration within an aqueous Ionic liquid. The effect of graphene nanoplatelets on the thermal conductivity properties of water and ethylene glycol-based nanofluids was explored by Gao, Wang [16]. The authors reported an increase in heat conductivity of up to 18% as a result of the addition of graphene nanoplatelet nanoparticles. In a recent investigation, MXene nanosheet is hybridized with  $\text{Al}_2\text{O}_3$  nanoparticles to synthesize MXene +  $\text{Al}_2\text{O}_3$  hybrid nanoparticles which was later dispersed into Therminol 55 (TH55) at three different concentrations of 0.05, 0.10, and 0.20 wt%. The formulated nanofluid had excellent dispersion stability without obvious sedimentation/agglomeration. Nevertheless, the thermal conductivity was maximally increased by 61.8% at 0.20 wt% loading of nanoparticles. The thermogravimetric analysis recommended that the formulated nanofluid is viable for the medium temperature range heat transfer application up to 250 °C [17]. Additionally, because MXene,  $\text{Al}_2\text{O}_3$  and Therminol55 are hydrophobic by nature, the resulting nanofluids are expected to exhibit remarkable dispersion stability.

Another popular approach of increasing the performance of heat exchangers is to interrupt the fluid flow passage by including inserts that create swirl/vortex flow, resulting in greater heat transfer due to the expanded flow path and mixing. Smithberg and Landis [18] pioneered the use of twisted tape (TT) inserts in tubes to enhance heat transfer in 1964. To date, various modifications to the geometry of the insert have been attempted to increase the heat exchanger's efficiency. Eiamsa-ard, Seemawute [19] investigated the effects of peripherally cut TT on heat transfer and hydraulic performance, which showed that the peripherally-cut TT was more effective in augmenting hydrothermal performance for laminar flow regimes than turbulent flow. However, the maximum performance factor of the insert-assisted heat exchanger was 4.88 and 1.29 for laminar and turbulent flow, respectively. Moreover, the depth ratio (DR) and width ratio (WR) have an inverse relationship to the heat transfer performance, as higher DR and lower WR are recommended for optimum performance. Hong, Du [20] studied the hydrothermal performance of sinusoidal rib tube (SRT) and spirally corrugated tube (SCT) heat exchangers with multiple twisted tapes (MTT). However, the maximum heat transfer enhancements reported using the combination of MTT and SRT were 87.2 %, which was higher than the 47.0 % reported using STC and SRT. Nonetheless, the pressure drop penalty was significant as a result of the increased blockage area. Apart from this, helically TT [21], coaxial

cross TT [22], delta wing tape [23], dimpled TT [24], extruded surface TT [25], ribbed spiky TT [26], delta-winglet tapes [27], coiled wire [28], wavy tape [29] were also investigated in several studies. The larger flow blockage caused by inserts in the tube reduces the overall hydrothermal efficiency of the heat exchanger, prompting researchers to investigate the combined effect of nanofluids and inserts. This combination promises a higher thermohydraulic efficiency of the heat exchanger due to the high flow rate, turbulence, and stronger thermophysical qualities. The nanofluid's stability is also maintained thanks to the swirl flow created by the inserts. Thus, the combination of nanofluids and inserts has been significant, and a slew of researchers have focused on this field in recent studies. Table 1 outlines recent developments in heat transfer augmentation of heat exchangers using nanofluids and inserts. Although numerous studies have been conducted to determine the influence of numerous geometrical inserts on hydrothermal performance when used in conjunction with a variety of nanofluids. Due to their lack of stability or thermal degradation at elevated temperatures, the majority of nanofluids are unsuitable in extreme atmospheric conditions. MXene, a class of two-dimensional nanocomposites, has recently garnered considerable interest due to their enhanced capacity to tune the thermophysical and optical properties of a wide variety of based fluids [30, 31, 32]. Additionally, MXene-based nanofluids are extremely customizable and have higher stability than typical nanofluids. However, no work evaluating the hydrothermal performance of new MXene-based nanofluids has been identified. Nevertheless, several models can be used to depict the complicated mechanisms for heat transfer enhancement, numerical simulation of nanofluid flow in heat exchanger remains a tough topic. Several studies on heat exchanger using a wide range of nanofluids and hybrid nanofluids have used the single-phase (homogeneous) model [33, 34]. However, the homogeneous model has been abandoned in favor of the two-phase mixture model for numerical simulation of nanofluids due to its inability to accurately describe the heat transfer mechanism of nanofluids [35, 36].

The goal of this research is to do the first-ever numerical assessment of the combined influence of a recently developed TH55/MXene + Al<sub>2</sub>O<sub>3</sub> nanofluid and an insert turbulator on heat transfer performance in a double pipe heat exchanger (DPHEX) with two-phase flow instead of conventional single-phase flow. The traditional twisted tape inserts are modified by the addition of various geometrical ribs. The inclusion of nanofluid boosted the heat transfer rate due to the higher heat transport property, and the ribbed insert amplified the turbulence, which improved the heat transfer rate even more. Thus, the ribbed insert and nanofluid combination increased the heat exchanger's hydrothermal performance. Finally, a comparison of different ribbed inserts and conventional TT is

**Table 1**

Summary of recent studies of different heat exchangers equipped with different insert turbulators and nanofluids.

Ref. and Year	System description & Insert Geometry	Nanofluids & Concentration	Flow Condition	Significance/Limitation
[37]; 2021	System Type: TPHE  Insert Type: TT (P = 0.080 m), Porous Plate, Ribs	WO <sub>3</sub> /water.  $\Phi = 0.5$ – $3.0$ vol%	Re = 2000– 6500	<ul style="list-style-type: none"> <li>• Rib inserts showed the optimum performance in terms of Nu and overall heat transfer coefficient.</li> <li>• The performance evaluation coefficient (PEC) is lower than 1 for each case, meaning that penalty in pressure drop overtook the enhancement due to pronounced friction introduced by the increased blockage area.</li> </ul>
[38]; 2021	System type: HTHE. Insert Type: Conical wire coils (converging, diverging, converging diverging) P/D = 2,3	Graphene/Water. $\Phi = 0.5, 0.75$ and $1$ wt%	Re = 4000– 27000	<ul style="list-style-type: none"> <li>• Diverging wire coils combined with 1 wt% of nanofluid exhibit the highest PEC at P/D = 2 and lowest Re = 6283</li> </ul>
[39]; 2020	System type: SPHE.  Insert Type: Twisted tape TR = 5, 10, 15	Fe <sub>3</sub> O <sub>4</sub> /vacuum pump oil $\Phi = 0.05, 0.2$ and $0.5$ vol%	Re = 20–330	<ul style="list-style-type: none"> <li>• The highest enhancement in Nu was 39.53% when 0.5% nanofluid flowed in the test tube with a twisted tape insert having a H/D ratio of 5.</li> </ul>
[40]; 2019	System type: Twisted HE. Insert Type: Y tape insert.	Al <sub>2</sub> O <sub>3</sub> /Water $\Phi = 0.01, 0.02$ and $0.03$ vol%	Re = 5000–20,000	<ul style="list-style-type: none"> <li>• Rigorous penalty in Pressure drop outshone the enhancement in Nu, which deteriorates the PEC of the system.</li> </ul>
[41]; 2018	System type: SPHE.  Insert Type: longitudinal strip insert. AR = 1, 2, 4	Nano diamond- nickel/Water  $\Phi = 0.1$ , and $0.3$ vol %	Re = 3000–22,000	<ul style="list-style-type: none"> <li>• For a 0.3 vol% of nanofluid and a Re = 22,000, the Nu is increased by 35.43% without the longitudinal strip insert and that was 93.30% when longitudinal strip insert (AR = 1) was incorporated.</li> <li>• The stability of the formulated nanofluid was not assessed, therefore raise a concern about their applicability.</li> </ul>
[42]; 2017	System type: SPHE. Insert Type: Twisted conical strip inserts (staggered and non-staggered alignments)	Ag/Water $\Phi = 2, 3, 4$ , and $5.0$ vol%	Re = 100 - 1500	<ul style="list-style-type: none"> <li>• Staggered alignment shows a higher PEC than non-staggered alignment. Besides, non-staggered alignment leads to more extreme nanoparticle migration compared to staggered alignment.</li> </ul>
[43]; 2016	System type: SPHE.  Insert Type: Longitudinal strip inserts. AR = 1, 2, 4, 12	MWCNT–Fe <sub>3</sub> O <sub>4</sub> / Water  $\Phi = 0.1$ and $0.3$ vol %	Re = 3000– 22000	<ul style="list-style-type: none"> <li>• The Highest Nu enhancement occurred when AR is minimum, Re and <math>\Phi</math> are maximum. Nanofluid alone contributed to 31.10 % enhancement in Nu, and that was 50.99 with the combined effect of nanofluid and insert.</li> <li>• The stability of nanofluids was not assessed.</li> </ul>
[44]; 2015	System type: DPHE (U bend). Insert Type: Helical tape inserts. P/D = 1, 2, 4, 5	Al <sub>2</sub> O <sub>3</sub> /Water $\Phi = 0.01$ and $0.03$ vol%	Re = 3000 - 30000	<ul style="list-style-type: none"> <li>• Using insert and nanofluid simultaneously, maximum 32.91% enhancement in Nu and 38% penalty in friction factor was noticed at Re = 30000, and P/D = 5 compared to that using water without insert.</li> </ul>

undertaken in order to determine the optimal insert design in terms of Nusselt number and pressure drop for turbulent flow regimes with widely varying Reynolds numbers (4000–20000).

## 2. Numerical methods

### 2.1. Physical model

Figure 1 depicts the schematic of the 3D domain of the insert fitted DPHEX, and geometrical configurations of different inserts of this current study. The system was made up of two 1000 mm long concentric hollow tubes. The material of the tube was considered to be aluminum. Table 2 shows the actual dimensions of the physical systems. The annuli side of the DPHEX has hot water flowing forward, while the tube side has cold TH55 or TH55/MXene + Al<sub>2</sub>O<sub>3</sub> nanofluid at 0.2 wt.% flowing backward to establish a counter flow mechanism. At 0.2 wt% concentration, TH55/MXene + Al<sub>2</sub>O<sub>3</sub> had the maximum specific value and thermal conductivity as demonstrated in our previous experiment [17]. Thus, the simulation in this study is chosen to use this concentration. The inserts are positioned inside the inner tube so that the ribs are inclined at an angle of 45° with the tube side fluid flow direction. The annuli side entrance velocity was constant with regard to a Re of 12000, whereas the velocity in the inner tube varied with respect to Re, ranging from 4000 to 20000. The current study's boundary conditions and assumptions are stated below.

Boundary conditions:

- Uniform velocity inlet at both inner tube (Re = 4000–20000) and outer tube (Re = 12000);
- Inlet temperature of the tube side 353 K and inlet temperature of the annuli (283 K);
- Zero pressure outlet at both inlet and outlet.
- Thermally isolated outer wall of the outer tube.
- Thermally coupled interfaces between walls.

Assumptions:

- The problem is steady state, and the fluid flow is incompressible.
- No-slip boundary wall condition.
- The flow regime is turbulent.
- Nanofluid has Newtonian behavior.
- The nanofluid flow is a two-phase flow.

#### 2.1.1. Governing equations

The numerical analyses were executed by applying the RNG  $k-\epsilon$  turbulence model for the three-dimensional turbulent flow with

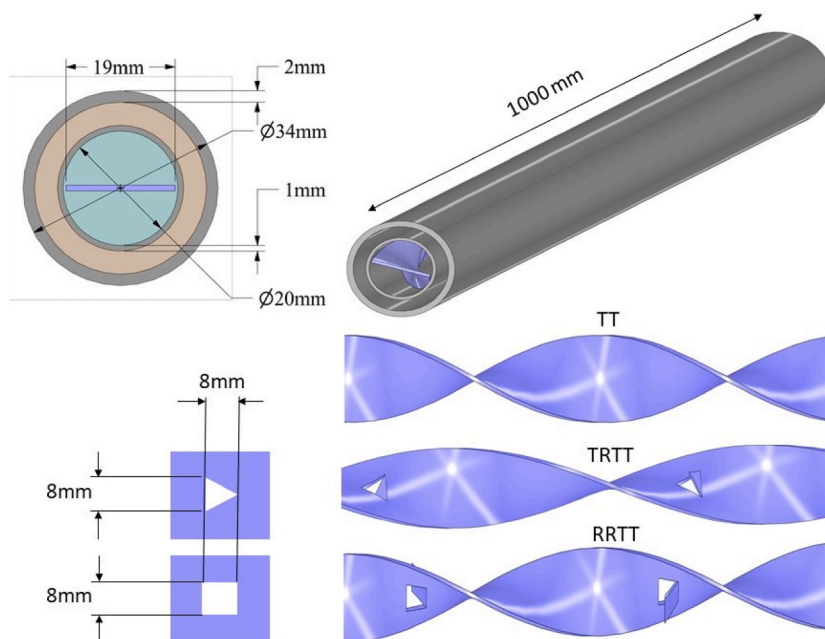


Figure 1. Geometry parameter definitions of the DPHEX, and different inserts used in this study.

**Table 2**  
Dimensions of different parameters of the DPHEX and inserts.

Parameter	Expression	Value
Outer tube length (mm)	L	1000
Outer tube inner diameter (mm)	D	30
Outer tube thickness (mm)	T	2
Inner tube length (mm)	l	1000
Inner tube inner diameter (mm)	d	20
Inner tube thickness (mm)	t	1
Tape width (mm)	w	19

Reynolds number (Re) ranging between 4000-20000. ANSYS 2020 R1-fluent (CFD) interface was associated in solving the governing equations (GEs) of continuity [Eqs. (1), (2), and (3)], momentum [Eqs. (4), (5), and (6)], energy [Eqs. (7), (8), (9), (10), (11), (12), and (13)], turbulent kinetic energy (k), and dissipation of energy (ε) [Eqs. (14), (15), (16), and (17)] [45, 46].

2.1.1.1. Continuity equation

$$\nabla(\rho_m \vec{U}_m) = 0 \tag{1}$$

$$\vec{U}_m = \frac{\rho_{(np)}\varphi_{(np)}\vec{U}_{(np)} + \rho_{bf}\varphi_{bf}\vec{U}_{bf} + \dots}{\rho_m} \tag{2}$$

$$\rho_m = \rho_{(np)}\varphi_{(np)} + \rho_{bf}\varphi_{bf} \tag{3}$$

here,  $\vec{U}_m$ , is the average mixed velocity, whereas  $\rho_m$  and  $\varphi$  denote the bulk density and concentration respectively.

2.1.1.2. Momentum equation

$$\rho_m(\vec{U}_m \nabla \vec{U}_m) = -\nabla \vec{P} + \mu_m \left( \nabla \vec{U}_m + (\nabla \vec{U}_m)^T \right) + \nabla \left( \rho_{bf}\varphi_{bf}\vec{U}_{dr,bf} + \rho_{(np)}\varphi_{(np)}\vec{U}_{dr,(np)} \right) + \rho_m \vec{g} \tag{4}$$

$$\vec{U}_{dr,bf} = \vec{U}_{bf} - \vec{U}_m \tag{5}$$

$$\vec{U}_{dr,(np)} = \vec{U}_{(np)} - \vec{U}_m \tag{6}$$

here,  $\mu_m$  represents average dynamic viscosity,  $\vec{U}_{dr,bf}$  and  $\vec{U}_{dr,(np)}$  are the drift velocity of the base fluid and hybrid NPs and  $\vec{g}$  is the gravitational constant.

2.1.1.3. Energy equation

$$\nabla(\rho_{bf}\varphi_{bf}\vec{U}_{bf}h_{bf} + \rho_{(np)}\varphi_{(np)}\vec{U}_{(np)}h_{(np)}) = \nabla((\varphi_{bf}k_{bf} + \varphi_{(np)}k_{(np)})\nabla T) \tag{7}$$

$$\nabla(\rho_{(np)}\varphi_{(np)}\vec{U}_m) = -\nabla(\rho_{(np)}\varphi_{(np)}\vec{U}_{dr,(np)}) \tag{8}$$

$$\vec{U}_{bf,(np)} = \vec{U}_{bf} - \vec{U}_{(np)}$$

$$\vec{U}_{dr,(np)} = \vec{U}_{(np),bf} - \frac{\rho_{(np)}\varphi_{(np)}\vec{U}_{bf,(np)}}{\rho_m} \tag{9}$$

$$\vec{U}_{bf,(np)} = \frac{d_p^2}{18\mu_{bf}f_d} \frac{\rho_{(np)} - \rho_{(np)}\vec{\alpha}}{\rho_{(np)}} \tag{10}$$

$$f_d = 1 + 0.15Re_{(np)}^{0.687} \tag{11}$$

$$\vec{\alpha} = \vec{g} - (\vec{U}_m \nabla \vec{U}_m) \tag{12}$$

$$Re_{(MXene:Al2O3)} = \frac{\vec{U}_m d_p \rho_m}{\mu_m} \tag{13}$$

here,  $Re$  is the Reynolds number,  $f_d$  is the drag function and  $\vec{\alpha}$  represents the acceleration.

2.1.1.4. Turbulence equation

$$\nabla(\rho_m \vec{U}_m k) = \nabla \left[ \left( \mu_m + \frac{\mu_{t,m}}{\sigma_k} \right) \nabla k \right] + G_{k,m} - \rho_m \varepsilon \tag{14}$$

$$\nabla(\rho_m \vec{U}_m \varepsilon) = \nabla \left[ \left( \mu_m + \frac{\mu_{t,m}}{\sigma_\varepsilon} \right) \nabla \varepsilon \right] + \frac{\varepsilon}{k} (C_1 G_{k,m} - C_2 \rho_m \varepsilon) \tag{15}$$

$$\mu_{t,m} = C_\mu \rho_m \frac{k^2}{\varepsilon} \tag{16}$$

$$G_{k,m} = \mu_{t,m} \left( \nabla \vec{U}_m - \left( \nabla \vec{U}_m \right)^T \right) \tag{17}$$

where,  $\mu_{t,m}$  is the turbulence dynamic viscosity,  $\varepsilon$  is the turbulent kinetic energy dissipation and the standard constants  $C_1 = 1.44$ ,  $C_\mu = 0.09$ ,  $G_{k,m} = 1.00$ ,  $C_2 = 1.92$ ,  $\sigma_k = 0.85$  and  $\sigma_\varepsilon = 1.30$  are used.

The thermophysical properties (thermal conductivity, viscosity, density, specific heat capacity) of TH55, MXene and  $Al_2O_3$  are accordance with your previous studies [17, 47].

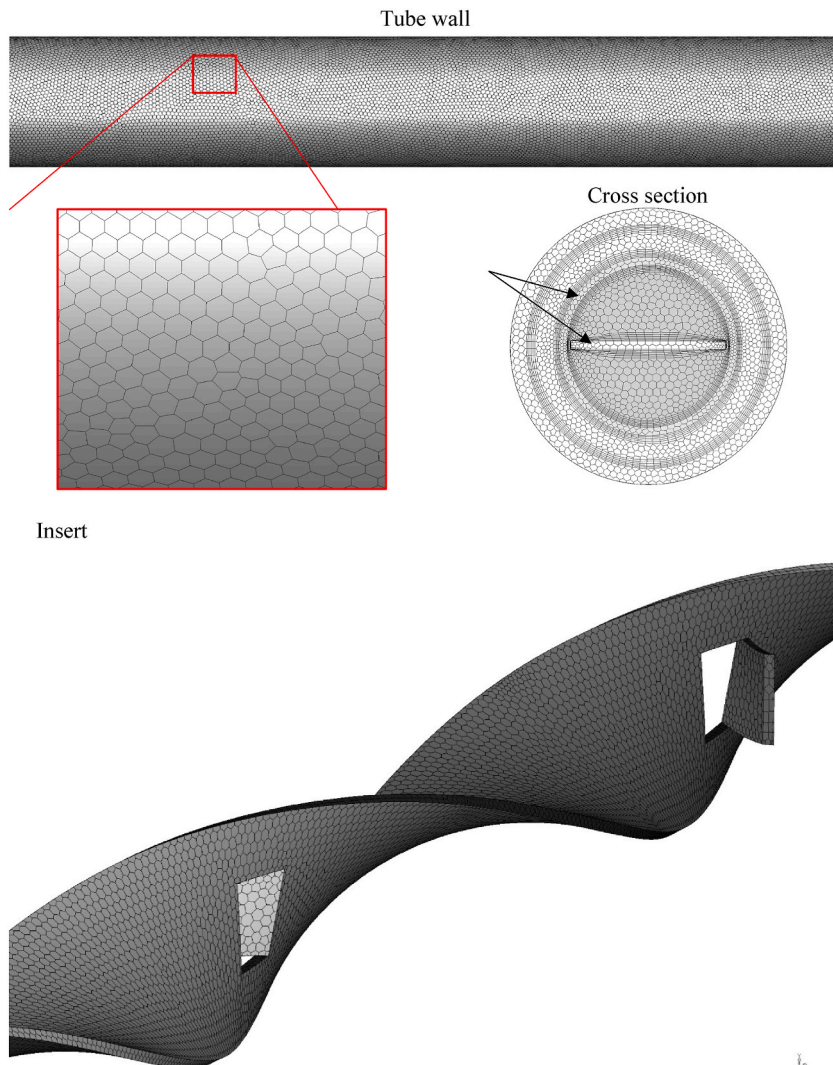


Figure 2. Meshing and grid generation in the computation domain of insert fitted DPHEX (a) inlet cross section; (b) outer tube; (c)TT insert.

### 2.1.2. Nanofluid properties and data reduction

The Nusselt number ( $Nu$ ) is a significant factor in fluid dynamics that represents the proportion of convective heat transfer to conductive heat transfer at a boundary within a fluid flow pattern. It can be computed using Eq. (18):

$$Nu = \frac{1}{A} \int Nu_x dA \quad (18)$$

where  $Nu_x$  is a local Nusselt number.

The friction factor ( $f$ ) is another crucial factor that has a significant impact on friction loss, heat transfer rate, and the efficiency of a heat exchanger. To calculate the friction factor, the Darcy-Weisbach equation is used, which relates it to the pressure drop ( $\Delta P$ ) across the tube length ( $L$ ) as shown in Eq. (19).

$$f = \frac{\Delta P}{\frac{L}{d} \left( \rho \frac{V^2}{2} \right)} \quad (19)$$

The evaluation of the performance of the system was conducted by taking into account the enhancement ratio of the Nusselt number and the frictional loss. This was used to calculate the performance evaluation coefficient (PEC) using Eq. (20).

$$PEC = \frac{\frac{Nu}{Nu_0}}{\left( \frac{L}{L_0} \right)^{\frac{1}{3}}} \quad (20)$$

### 2.1.3. Meshing and grid sensibility study

Figure 2 (a-c) depicts the meshing of the physical system. Mosaic meshing was used to discretize the computational domain in the current study. This is because mosaic meshing has an advantage over hexahedron or prismatic meshing in that it requires less computing time while maintaining the precision of the outputs [48]. In order to depict the viscous sublayer influence of turbulent flows, inflation layers with a growth rate of 1.2 are assigned between the fluid domain's solid-liquid interfaces. A second-order upwind spatial discretization scheme was applied to solve momentum, energy turbulent kinetic energy with SIMPLE pressure-velocity coupling algorithm. In order to obtain the convergency of the continuity, momentum, energy,  $k$ , and  $\epsilon$  equations, the absolute criteria of residuals were set to  $10^{-6}$ . The grid sensibility was assessed for varying number of elements size with respect to the  $Nu$  and  $f$  as depicted in Table 3. When the element number reached 969960 the deviations were below 0.007% and 0.12% for  $Nu$  and  $f$ , respectively; thereby, the mesh corresponding to 969960 element number was chosen for all simulations.

### 2.1.4. Model validation

The current simulation's validity was confirmed by comparing the numerical values of the  $Nu$  and  $f$  with two well-established empirical correlations for the smooth pipe. For example, the Dittus and Boelter model [49] is used to validate  $Nu$ , whereas the Blasius model [49]) is utilized to validate  $f$ . Figure S1 depicts the validation outcomes which clearly shows that the relative variations between the correlation output are quite minimal, usually within 5% of the deviation line. Apart from the present model shows good agreements with the experimental values studied by [50]. As a result, the validation of this model confirms the acceptable discrepancies in the current simulations.

## 3. Results and discussion

### 3.1. Effect of insert on flow characteristics

The inclusion of TH55/MXene +  $Al_2O_3$  and ribbed insert both have significant impact on the flow streamlines. The streamlines along the flow direction are presented in Figure 3a for the smooth tube and tube equipped with inserts. In the case of a smooth tube, the velocity streamline is in the axial direction. The twisted tape insert, on the other hand, generates a swirl motion, which guided the fluid motion into the radial and tangential directions. As indicated by the cross-sectional velocity streamline (Figure 3b), the twisted tape divides the fluid flow into two helical compartments on either side of the insert. Each compartment has similar velocity streamlines, but they flow in opposing directions toward the circumference. Nevertheless, the velocity streamlines are further influenced due to the

**Table 3**  
Grid sensibility test of the DPHEX for plain tube and with nanofluid at  $Re = 20000$ .

Element Number	$Nu$	%Deviation	$f$	%Deviation
155838	126.584	-	0.03459	
183576	128.565	1.564969	0.03045	13.60
287180	129.589	0.796484	0.02842	7.14
465985	129.701	0.086427	0.02785	2.04
635403	129.736	0.026985	0.02763	0.79
969960	129.745	0.006937	0.02760	0.11
1557575	129.749	0.003083	0.02759	0.04

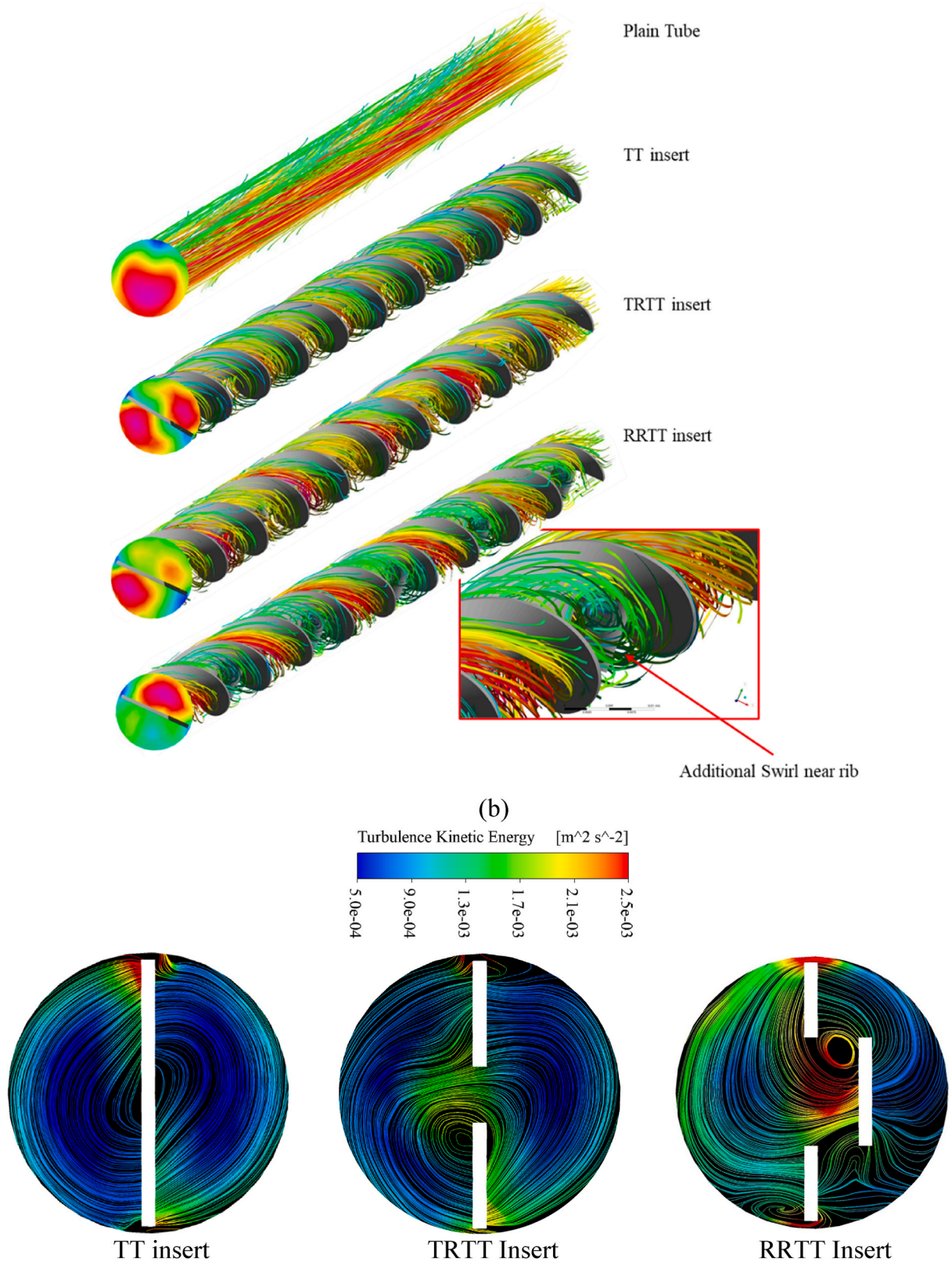


**Figure 3.** Velocity Streamline of the TH55/MXene + Al<sub>2</sub>O<sub>3</sub> flowing (a) along the path inside the inner pipe for plain tube and different geometrical inserts at Re = 4000, (b) Variation in cross-sectional velocity streamline for different inserts.

additional flow disturbance caused by the ribs on TT. As shown in Figure 3a, additional swirl motion is generated near the ribbed area of the insert while comparing with conventional TT insert. Consequently, the cross-sectional velocity profiles of the ribbed insert are altered from the conventional TT insert. Additional vortices are introduced near the ribs for both the TRTT and RRTT inserts, unlike the conventional TT insert. The vortices in the RRTT insert, on the other hand, appear to be more intensified, which could be attributable to the fact that the fluid encounters a larger blockage ratio than in the TRTT insert [51, 52].

The velocity profile of the fluid was significantly altered when different types of Inserts were used, as shown in Figure 4(a-e). For example, in the case of a plain tube fluid flow, the velocity gradient forms a heart-like shape with a maximum velocity zone in the core, whereas in the case of a TT inserted tube, two similar velocity gradients are formed at each compartment, which take the shape of an aero foil with a maximum velocity zone in the central core. Nonetheless, the aero foil form that was established in the case of the TT insert was disturbed by introducing ribs into the TT insert, resulting in the formation of two separate zones on either side of the tape. The velocity on the ribbed side is significantly lower and the velocity gradient is less pronounced than the rib-free side of the insert. This is attributed to the enlarged turbulence kinetic energy in the ribbed side of the tube [53, 54]. When comparing the velocity

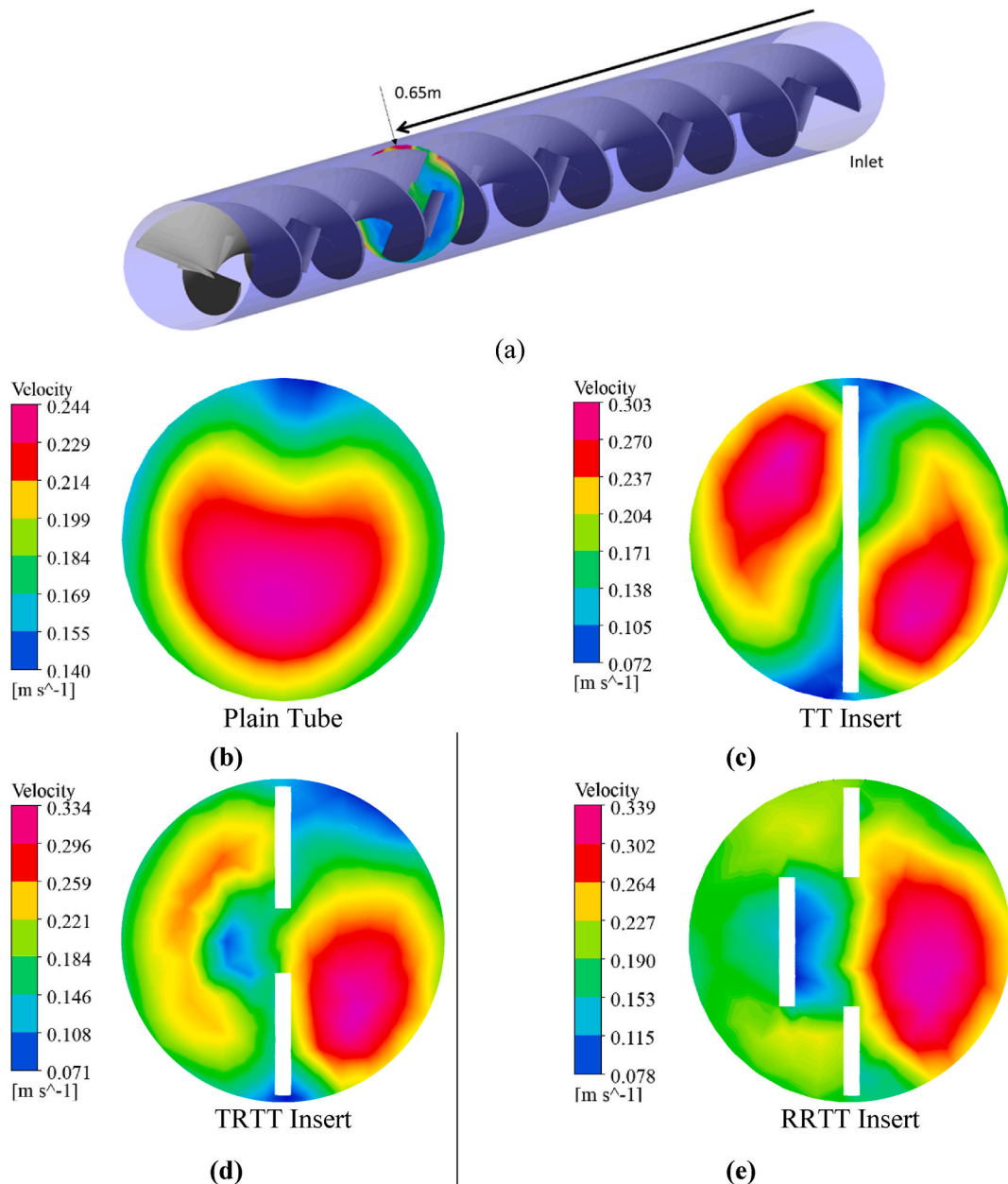


**Figure 4.** (a) Axial cross sectional velocity profile at a distance 0.65 m from the inlet for (b) Plain tube, tube with (c) TT insert, (d) TRTT insert and (e) RRTT insert.

profiles, it's evident that RRTT inserts have a greater maximum velocity than TT and TRTT inserts, which is owing to the RRTT insert's larger blockage ratio than other types of inserts [54]. Therefore, the velocity gradient is more observable in the case of RRTT inserts tube than other types of geometry. The TT insert generates swirl motion resulting from the radial,  $V_r$  and tangential,  $V_t$  velocity of the fluid. The  $V_t$  and  $V_r$  profile are illustrated in Figure 5(a–f) for different types of inserts. It can be noticed from the figure that the tangential and radial velocity are higher in the RRTT insert than in the TT and TRTT inserts. Therefore, the RRTT insert provides more turbulence compared to conventional TT and TRTT inserts. Nevertheless, it is expected that the heat transfer will be intensified

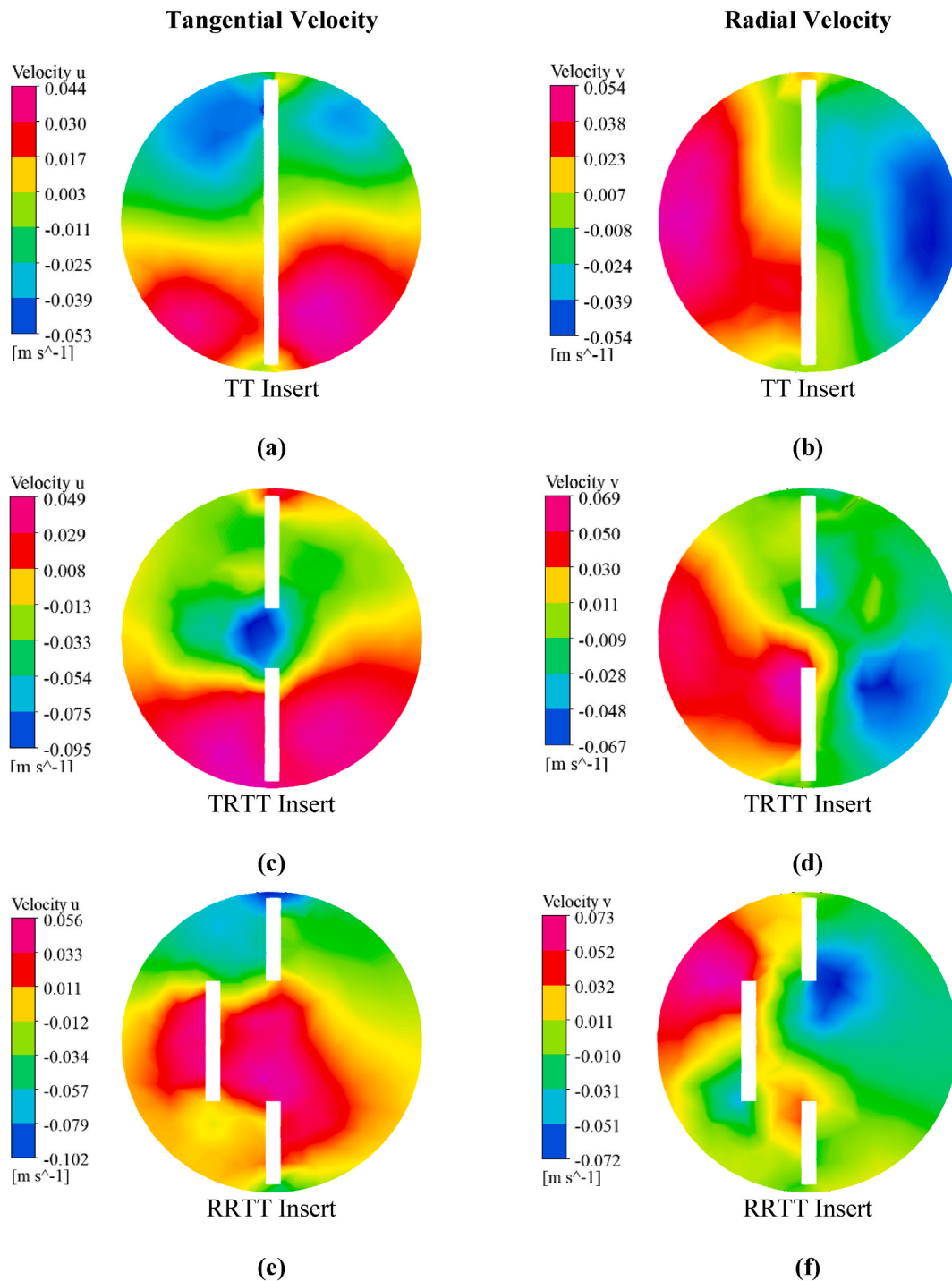


**Figure 5.** Tangential and Radial velocity profile at the cross-section at a distance 0.65 m from the inlet for (a–b) TT insert, (c–d) TRTT insert (e–f) RRTT insert.

between the solid wall and fluid layer due to the higher turbulence intensity [55]. In addition, the thermal boundary layer will be thinner in RRTT inserted tubes compared to the other two types of inserts [56].

Figure 6(a–d) shows the temperature at the outlet cross section for various inserted tubes as well as plain tubes. The swirl intensity for the RRTT insert is highest when compared to the TRTT and traditional TT inserts, resulting in a more uniform temperature distribution, as shown by the temperature contour. This is due to the increased fluid path and better fluid mixing caused by the generated centrifugal force, which results in a high tangential velocity. The RRTT insert's outlet temperature is marginally higher than the TT and TRTT inserts, as shown in temperature contours. This is attributed to the thinnest boundary layer caused by the highest turbulence intensity as compared to TRTT and TT insert. On the other hand, the temperature gradients on both sides of the TT insert are identical, whereas those on the TRTT and RRTT inserts are separated into zones of higher and lower temperature gradients. This phenomenon results from the differences in fluid turbulence on each side of the insert. The inlet pressure drop, which represents the total pressure drop along the total flow path, is significantly altered by the inserts, as evidenced by the pressure contours in Figure 7(a–d). The addition of TT substantially quadrupled the total pressure drop compared to the plain tube. The ribs provided additional resistance to the fluid flow channel, resulting in a larger pressure drop than a standard TT insert. However, due to the higher disturbance generated by the fluid in the RRTT insert than in other insert shapes, the maximum pressure drop was perceptible. As a result, the average friction factor for the RRTT insert is expected to be greater, which may increase pumping costs. In other words, the production of a stronger secondary axial flow enhances both the heat transfer rate and the pressure drop, which are both a result of higher fluid momentum.

### 3.2. Effect of nanofluid on flow characteristics

The streamlines for nanofluid and base fluid are identical, as shown in Figure S2 (Supplementary Documents), indicating that substituting nanofluid for TH55 has no effect on the fluid streamline. However, the nanofluid's output temperature is greater than that of TH55, indicating that heat transfer rate improved employing nanofluid over TH55. The increased heat transfer rate between the tube wall and nanofluid is attributed to the higher thermal conductivity of TH55/MXene + Al<sub>2</sub>O<sub>3</sub> due to the inclusion of MXene nanoparticles. Despite this, the overall pressure drop is higher when utilizing TH55 + MXene nanofluid, which may be ascribed to the

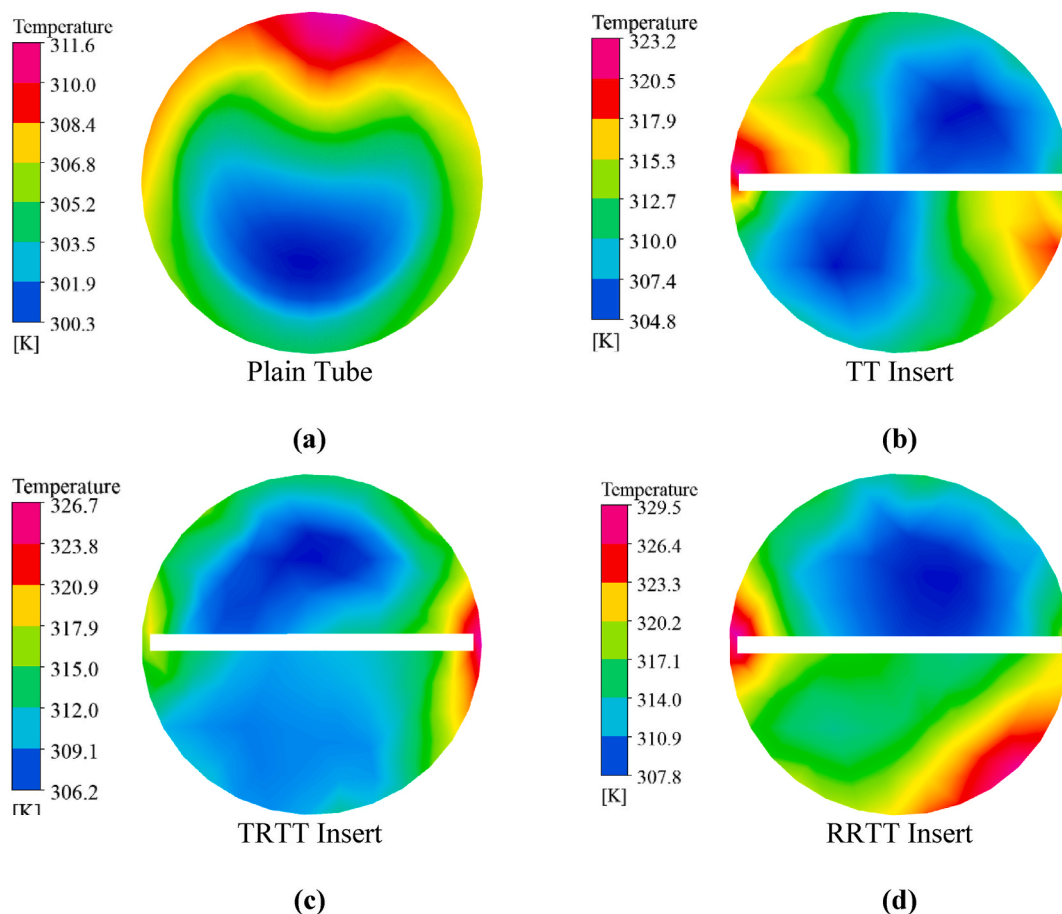


**Figure 6.** Outlet temperature profile for different inserts at  $Re = 20000$  with TH55/MXene + Al<sub>2</sub>O<sub>3</sub> for (a) Plain Tube (b) TT Insert (c) TRTT Insert, and (d) RRTT insert.

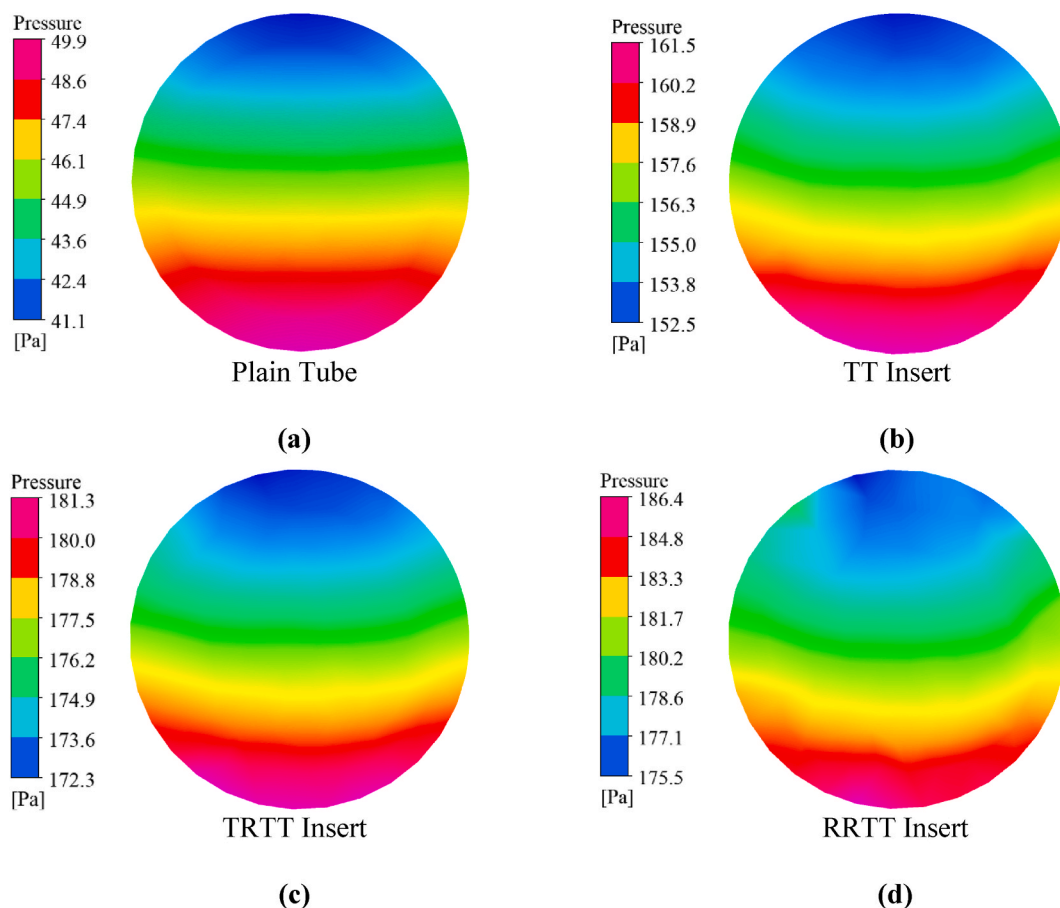


**Figure 7.** Inlet pressure (considering zero pressure outlet) contour for different inserts at  $Re = 20000$  with TH55/MXene +  $Al_2O_3$  for (a) Plain Tube (b), TT Insert (c) TRTT Insert, and (d) RRTT insert.

increased viscosity of the nanofluid as previously defined. The effect of increasing viscosity has a modest influence on flow velocity.

### 3.3. Nusselt Number, friction factor and performance evaluation criterion

The thermohydraulic performance of this current study is investigated in terms of Nusselt Number ( $Nu$ ), friction factor ( $f$ ) and overall performance of the system is analyzed in terms of PEC. The obtained  $Nu$  from Eq. (19) and the ratio of  $Nu$  are plotted in Figure 8 (a-d) to show the effect of TH55/MXene +  $Al_2O_3$  nanofluid together with different geometrical inserts at varying  $Re$  from 4000-20000. It can be observed that the average  $Nu$  of 0.2 wt.% TH55/Mxene +  $Al_2O_3$  nanofluid is higher than that of TH55 flowing inside the annuli for all ribbed inserts, and a maximum of 11.04% enhancement in  $Nu$  is obtained at  $Re = 20000$  compared to water. While comparing the effect of various inserts on the  $Nu$ , it is clear that all types of inserts demonstrate a greater  $Nu$  value than plain tubes. The Nusselt number tends to increase almost linearly as  $Re$  increases. The  $Nu$  augmentation in rectangular ribbed TT, on the other hand, was more pronounced than in TT and triangular-ribbed TT. This might be attributable to the increased hydrothermal characteristics indicated in the temperature and axial velocity contours in Figures 5, 6, 7, and 8, respectively. The enhancement ratio in the Nusselt number ranges between 1.1 -1.9 with TH55 base fluid and 1.25–2.05 with nanofluid. Maximum enhancement was observed for both base fluid and nanofluid at  $Re = 4000$ , whereas  $Nu_{insert}/Nu_{plain}$  tube becomes approximately similar in magnitude at  $Re = 20000$ , meaning that the efficacy of ribbed geometry decreases as  $Re$  increases.

The  $f$  and ratio of friction factor,  $f/f_{plain}$  tube as a function of  $Re$  are plotted in Figure 9 (a-d) for different insert geometries. The plots reveal that with the increase in  $Re$ , the friction factor significantly drops, consistent with the previous study [57]. However, the friction factor for each type of insert is reported to be high when compared to the plain tube. The blockage in the ribbed TT increased the friction factor compared to conventional TT inserts, and the RRTT encountered the maximum friction factor as illustrated in Figure 9 (c-d). Furthermore, the impact of utilizing a nanofluid other than TH55 demonstrates that the friction factor for TH55-based nanofluid is somewhat higher than for TH55 across the temperature range investigated. The increased friction factor of the nanofluid is due to the higher viscosity with nanofluid compared to pure TH55. Furthermore,  $Re$  has a strong influence on lowering the friction factor of nanofluids, indicating that the differences in friction coefficient between various inserts are negligible near  $Re = 20000$ . This is also

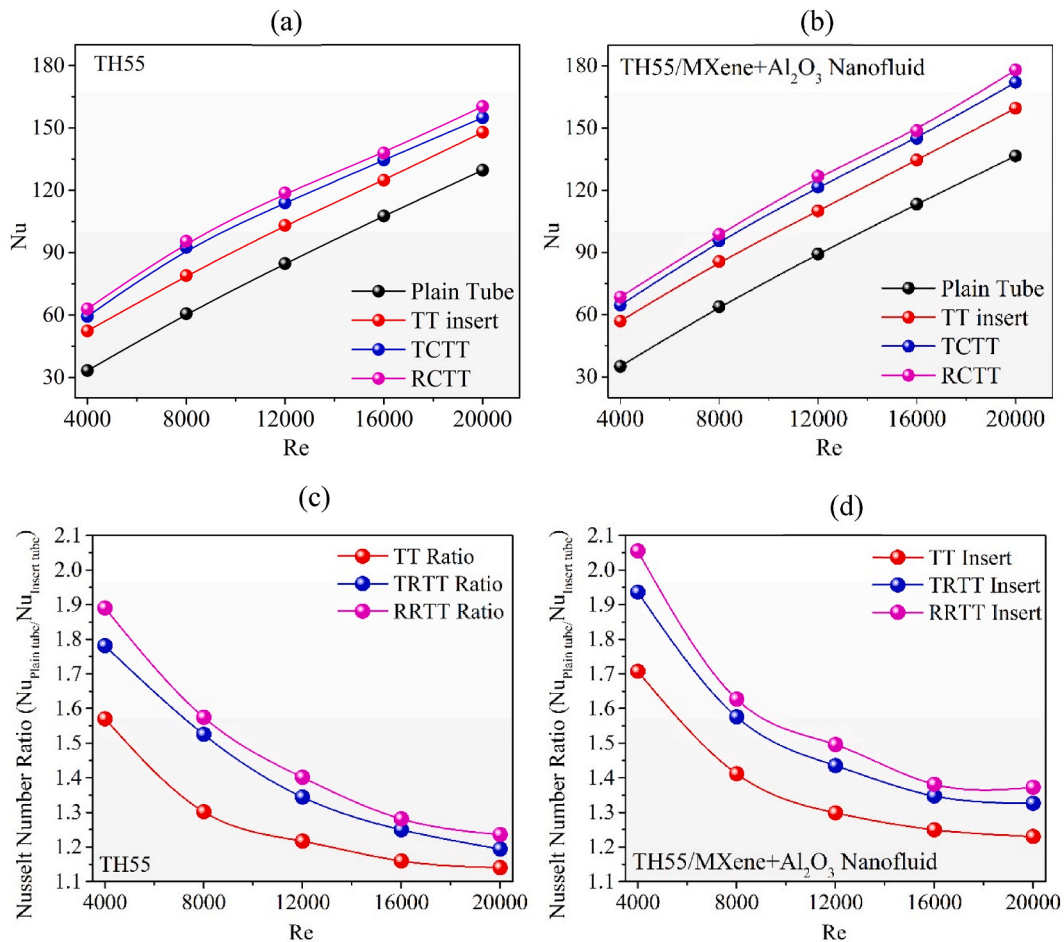


**Figure 8.** Nu as a function of Re for different inserts (a) with base fluid, (b) with nanofluid. The ratio of Nu for different inserts with (c) base fluid, (d) with nanofluid.

obvious from the trend that the friction factor becomes nearly constant as the Re increased. In consistent with these present studies similar findings can be observed in literature [58, 59] However, at  $Re = 4000$ , the maximum value friction factor ratio is 1.8 for rectangular-ribbed TT, whereas the values for TRTT and conventional TT insert are 1.72 and 1.45, respectively.

Since incorporations of nanofluid and inserts significantly improve the heat transfer rate of the system, simultaneously the increase the pumping power resulting from higher frictional coefficient. As a result, they have both positive and negative impacts on the overall performance of the thermal system. Therefore, it is crucial to check the performance of the DPHEX bringing both the heat transfer augmentation and frictional penalty together. As we noticed before the incorporation of inserts and nanofluid simultaneously enhanced the Nu and friction factor for all cases. Therefore, for a better comparison, the performance evaluation coefficient (PEC) was assessed using Eq. (20), as illustrated in Figure 10. The magnitude of the PEC is greater than 1 in all cases, suggesting that the positive impact of heat transfer enhancement outweighs the negative impact of frictional pressure drop. The rectangular-ribbed TT insert has a maximum PEC of 1.56 at  $Re = 4000$  when TH55 is used as the working fluid (Figure 10a), and this is further increased to 1.67 when TH55/MXene + Al<sub>2</sub>O<sub>3</sub> nanofluid is used replacing TH55 (Figure 10b). This result demonstrates that the insert in all configurations has an advantageous effect on total heat transfer performance. However, at high Re, the PEC deteriorates as the Nu enhancement rate becomes shallow with increasing Re. Nevertheless, the friction factor drops at a lower rate at high Re. Therefore, better heat transfer performance can be obtained at lower Re. To compare our outcome with other studies from literature, the PEC of this studies with RRTT insert outperformed many other types of inserts, for instance, ribbed and grooved wire coils with  $PEC = 1.36$  [60]; equilateral triangle coiled wire with  $PEC = 1.37$  [61]; Tandem Wire Coil Element Insert with  $PEC = 1.26$  [62].

#### 4. Concluding remarks

The current study aims to improve the hydrothermal performance of a double pipe heat exchanger by combining the effects of a newly synthesized TH55/MXene + Al<sub>2</sub>O<sub>3</sub> nanofluid with various geometrically ribbed inserts for the turbulent flow regime ( $Re$  4000–20000). A two-phase numerical model was considered to obtain hydrothermal performance of DPHEX. The significant outcomes

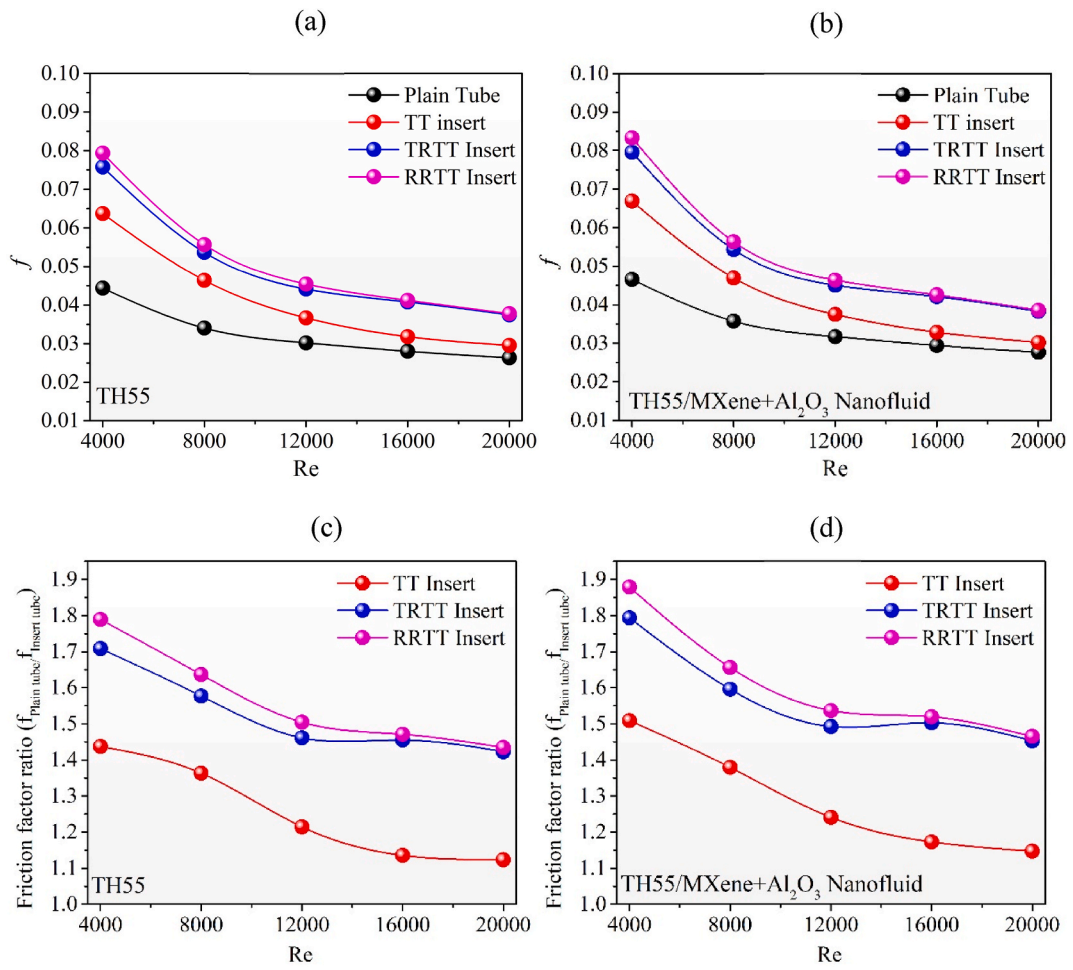


**Figure 9.** The  $f$  as a function of  $Re$  for different inserts (a) with base fluid, (b) with nanofluid. The ratio of  $f$  for different inserts with (c) base fluid, (d) with nanofluid.

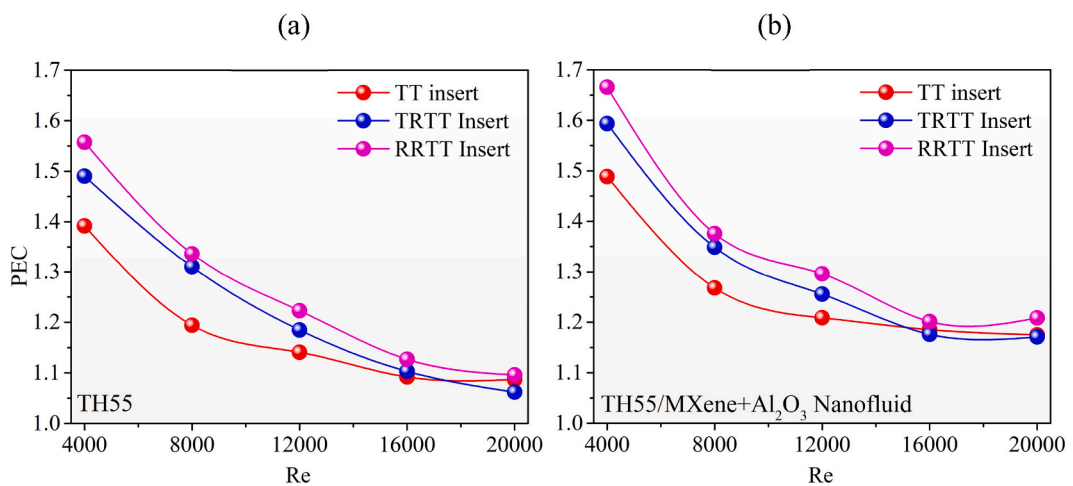


**Figure 10.** PEC vs.  $Re$  of DPHE for different inserts with (a) TH55 Base fluid (b) TH55/MXene + Al<sub>2</sub>O<sub>3</sub> nanofluid.

of this study are summarized below:

- The inclusion of ribbed (rectangular, triangular) inserts increases turbulence by generating sufficient vortices in addition to the traditional TT insert. As a result of the increased axial and radial velocity, the thermal boundary layer becomes thinner. Owing to the large flow blockage encountered by the flowing fluid, the total pressure drop between the inlet and outlet is increased by adding ribs.
- The maximum enhancement in Nu is recorded to be 11.04%. It was observed using TH55/MXene + Al<sub>2</sub>O<sub>3</sub> nanofluid as a replacement of base fluid, and the combination of insert and nanofluid showed up to 105% enhancement for rectangular-ribbed TT in Nu as compared to the plain tube with TH55 as the working fluid.
- The rectangular-ribbed TT had the worst pressure drop because of the high flow disturbance. TT and triangular-ribbed TT also had the worst pressure drop.
- Despite the fact that the RRTT insert has a maximum penalty in pressure drop, the PEC assessment shows that the RRTT insert has a maximum performance factor of 1.67 higher than 1.61 for TRTT and 1.49 for conventional TT insert incorporating nanofluid. On the other hand, using TH55 as the working fluid, the corresponding values are 1.56, 1.48, and 1.39 for RRTT, TRTT, and conventional TT, respectively.

#### Author contribution statement

LineNoBookmarkStart:ID:243 = = Name:Line\_euclid3592121739\_87].

Likhan Das; Navid Aslfattahi: Conceived and designed the experiments; Performed the experiments; Analyzed and interpreted the data; Contributed reagents, materials, analysis tools or data; Wrote the paper.

Khairul Habib; R.Saidur; Kumaran Kadirgama: Analyzed and interpreted the data; Contributed reagents, materials, analysis tools or data; Wrote the paper.

Anupom Das: Performed the experiments; Analyzed and interpreted the data; Contributed reagents, materials, analysis tools or data; Wrote the paper.

#### Funding statement

Prof Kumaran Kadirgama was supported by Universiti Malaysia Pahang [RDU213308].

#### Data availability statement

Data will be made available on request.

#### Additional information

Supplementary content related to this article has been published online at <https://doi.org/10.1016/j.heliyon.2023.e14283>.

#### Declaration of interest's statement

The authors declare no competing interests.

#### References

- [1] D. Triché, et al., Experimental and numerical study of a falling film absorber in an ammonia-water absorption chiller, *Int. J. Heat Mass Tran.* 111 (2017) 374–385.
- [2] Y. Cao, et al., Thermo-economic evaluation of a combined Kalina cycle and humidification-dehumidification (HDH) desalination system integrated with thermoelectric generator and solar pond, *Int. J. Heat Mass Tran.* 168 (2021) 120844.
- [3] J. Yu, et al., Investigation on heat transfer characteristics of outside heat exchanger in an air conditioning heat pump system for electric vehicles, *Int. J. Heat Mass Tran.* 170 (2021) 121040.
- [4] F. Rubbi, et al., Performance optimization of a hybrid PV/T solar system using Soybean oil/MXene nanofluids as A new class of heat transfer fluids, *Sol. Energy* 208 (2020) 124–138.
- [5] S.U. Choi, J.A. Eastman, *Enhancing thermal Conductivity of Fluids with Nanoparticles*, Argonne National Lab., IL (United States), 1995.
- [6] S.K. Singh, J. Sarkar, Hydrothermal performance comparison of modified twisted tapes and wire coils in tubular heat exchanger using hybrid nanofluid, *Int. J. Therm. Sci.* 166 (2021) 106990.
- [7] S.K. Singh, J. Sarkar, Experimental hydrothermal characteristics of concentric tube heat exchanger with V-cut twisted tape turbulator using PCM dispersed mono/hybrid nanofluids, *Exp. Heat Tran.* 34 (5) (2021) 421–442.
- [8] J. Albadr, S. Tayal, M. Alasadi, Heat transfer through heat exchanger using Al<sub>2</sub>O<sub>3</sub> nanofluid at different concentrations, *Case Stud. Therm. Eng.* 1 (1) (2013) 38–44.
- [9] F. Afshari, et al., Heat transfer enhancement of finned shell and tube heat exchanger using Fe<sub>2</sub>O<sub>3</sub>/water nanofluid, *J. Cent. S. Univ.* 28 (11) (2021) 3297–3309.
- [10] F. Afshari, B. Muratçobanoğlu, Thermal analysis of Fe<sub>3</sub>O<sub>4</sub>/water nanofluid in spiral and serpentine mini channels by using experimental and theoretical models, *Int. J. Environ. Sci. Technol.* (2022).

- [11] S.K. Singh, J. Sarkar, Improving hydrothermal performance of hybrid nanofluid in double tube heat exchanger using tapered wire coil turbulator, *Adv. Powder Technol.* 31 (5) (2020) 2092–2100.
- [12] M. Fares, M. Al-Mayyahi, M. Al-Saad, Heat transfer analysis of a shell and tube heat exchanger operated with graphene nanofluids, *Case Stud. Therm. Eng.* 18 (2020) 100584.
- [13] V. Kumar, A.K. Tiwari, S.K. Ghosh, Effect of variable spacing on performance of plate heat exchanger using nanofluids, *Energy* 114 (2016) 1107–1119.
- [14] N. Aslfattahi, et al., MXene based new class of silicone oil nanofluids for the performance improvement of concentrated photovoltaic thermal collector, *Sol. Energy Mater. Sol. Cell.* 211 (2020) 110526.
- [15] L. Das, et al., Improved thermophysical properties and energy efficiency of aqueous ionic liquid/MXene nanofluid in a hybrid PV/T solar system, *Nanomaterials* 10 (7) (2020) 1372.
- [16] Y. Gao, et al., Measurement and modeling of thermal conductivity of graphene nanoplatelet water and ethylene glycol base nanofluids, *Int. J. Heat Mass Tran.* 123 (2018) 97–109.
- [17] L. Das, et al., Thermo-optical Characterization of Therminol55 based MXene–Al<sub>2</sub>O<sub>3</sub> hybridized Nanofluid and new Correlations for thermal properties, *Nanomaterials* (11) (2022) 12.
- [18] E. Smithberg, F. Landis, Friction and Forced Convection Heat-Transfer Characteristics in Tubes with Twisted Tape Swirl Generators, 1964.
- [19] S. Eiamsa-ard, P. Seemawute, K. Wongcharee, Influences of peripherally-cut twisted tape insert on heat transfer and thermal performance characteristics in laminar and turbulent tube flows, *Exp. Therm. Fluid Sci.* 34 (6) (2010) 711–719.
- [20] Y. Hong, et al., Thermal-hydraulic performances in multiple twisted tapes inserted sinusoidal rib tube heat exchangers for exhaust gas heat recovery applications, *Energy Convers. Manag.* 185 (2019) 271–290.
- [21] K.L. Liaw, J.C. Kurnia, A.P. Sasmito, Turbulent convective heat transfer in helical tube with twisted tape insert, *Int. J. Heat Mass Tran.* 169 (2021) 120918.
- [22] X. Liu, et al., Numerical analysis on enhanced performance of new coaxial cross twisted tapes for laminar convective heat transfer, *Int. J. Heat Mass Tran.* 121 (2018) 1125–1136.
- [23] A.T. Wijayanta, et al., Double-sided delta-wing tape inserts to enhance convective heat transfer and fluid flow characteristics of a double-pipe heat exchanger, *Appl. Therm. Eng.* 145 (2018) 27–37.
- [24] L. Zheng, Y. Xie, D. Zhang, Numerical investigation on heat transfer performance and flow characteristics in circular tubes with dimpled twisted tapes using Al<sub>2</sub>O<sub>3</sub>-water nanofluid, *Int. J. Heat Mass Tran.* 111 (2017) 962–981.
- [25] F. Rubbi, et al., Numerical Study of Heat Transfer Enhancement of Turbulent Flow Using Twisted Tape Insert Fitted with Hemispherical Extruded Surface 38, 2020, pp. 314–320.
- [26] S.W. Chang, B.J. Huang, Thermal performances of tubular flows enhanced by ribbed spiky twist tapes with and without edge notches, *Int. J. Heat Mass Tran.* 73 (2014) 645–663.
- [27] M. Khoshvaght-Aliabadi, et al., Experimental and numerical studies of air flow and heat transfer due to insertion of novel delta-winglet tapes in a heated channel, *Int. J. Heat Mass Tran.* 169 (2021) 120912.
- [28] H.A. Moghaddam, A. Sarmadian, M. Shafaei, An experimental study on condensation heat transfer characteristics of R-600a in tubes with coiled wire inserts, *Appl. Therm. Eng.* 159 (2019) 113889.
- [29] Y. Liang, et al., Numerical investigation of heat transfer and flow characteristics of laminar flow in a tube with center-tapered wavy-tape insert, *Appl. Therm. Eng.* 148 (2019) 557–567.
- [30] K. Kadirgama, et al., Experimental investigation on the optical and stability of aqueous ethylene glycol/mxene as a promising nanofluid for solar energy harvesting, *IOP Conf. Ser. Mater. Sci. Eng.* 1062 (1) (2021) 12022.
- [31] N. Parashar, et al., ANN Modeling of thermal Conductivity and Viscosity of MXene-based aqueous IoNanofluid, *Int. J. Thermophys.* 42 (2) (2021) 24.
- [32] L. Samyilingam, et al., Thermal and energy performance improvement of hybrid PV/T system by using olein palm oil with MXene as a new class of heat transfer fluid, *Sol. Energy Mater. Sol. Cell.* 218 (2020) 110754.
- [33] H.A. Mohammed, P. Gunnasegaran, N.H. Shuaib, Heat transfer in rectangular microchannels heat sink using nanofluids, *Int. Commun. Heat Mass Tran.* 37 (10) (2010) 1496–1503.
- [34] Y.-T. Yang, H.-W. Tang, W.-P. Ding, Optimization design of micro-channel heat sink using nanofluid by numerical simulation coupled with genetic algorithm, *Int. Commun. Heat Mass Tran.* 72 (2016) 29–38.
- [35] V. Kumar, J. Sarkar, Two-phase numerical simulation of hybrid nanofluid heat transfer in minichannel heat sink and experimental validation, *Int. Commun. Heat Mass Tran.* 91 (2018) 239–247.
- [36] V. Kumar, J. Sarkar, Numerical and experimental investigations on heat transfer and pressure drop characteristics of Al<sub>2</sub>O<sub>3</sub>-TiO<sub>2</sub> hybrid nanofluid in minichannel heat sink with different mixture ratio, *Powder Technol.* 345 (2019) 717–727.
- [37] A.K. Tiwari, et al., Experimental and numerical investigation on the thermal performance of triple tube heat exchanger equipped with different inserts with WO<sub>3</sub>/water nanofluid under turbulent condition, *Int. J. Therm. Sci.* (2021) 106861.
- [38] O. Keklikcioglu, V. Ozceyhan, Thermohydraulic performance evaluation for horizontal tube by using combination of modified coiled wire inserts and graphene nanoplatelet-water nanofluids, *Int. Commun. Heat Mass Tran.* 123 (2021) 105206.
- [39] L.S. Sundar, et al., Augmentation of Heat Transfer of High Prandtl Number Fe<sub>3</sub>O<sub>4</sub>/vacuum pump oil nanofluids flow in a tube with twisted tape inserts in laminar flow, *Heat Mass Tran.* 56 (11) (2020) 3111–3125.
- [40] M. Omid, A.A. Rabienataj Darzi, M. Farhadi, Turbulent heat transfer and fluid flow of alumina nanofluid inside three-lobed twisted tube, *J. Therm. Anal. Calorim.* 137 (4) (2019) 1451–1462.
- [41] L. Syam Sundar, M.K. Singh, A.C.M. Sousa, Heat transfer and friction factor of nanodiamond-nickel hybrid nanofluids flow in a tube with longitudinal strip inserts, *Int. J. Heat Mass Tran.* 121 (2018) 390–401.
- [42] R. Mashayekhi, et al., Application of a novel conical strip insert to improve the efficacy of water–Ag nanofluid for utilization in thermal systems: a two-phase simulation, *Energy Convers. Manag.* 151 (2017) 573–586.
- [43] L. Syam Sundar, et al., Heat transfer and friction factor of multi-walled carbon nanotubes–Fe<sub>3</sub>O<sub>4</sub> nanocomposite nanofluids flow in a tube with/without longitudinal strip inserts, *Int. J. Heat Mass Tran.* 100 (2016) 691–703.
- [44] P.V. Durga Prasad, et al., Experimental study of heat transfer and friction factor of Al<sub>2</sub>O<sub>3</sub> nanofluid in U-tube heat exchanger with helical tape inserts, *Exp. Therm. Fluid Sci.* 62 (2015) 141–150.
- [45] A. Aghaei, et al., Heat transfer and fluid flow analysis using nanofluids in diamond-shaped cavities with novel obstacles, *Eng. Appl. Comp. Fluid Mechanics* 15 (1) (2021) 1034–1056.
- [46] A. Salari, et al., Nanofluid based photovoltaic thermal systems integrated with phase change materials: numerical simulation and thermodynamic analysis, *Energy Convers. Manag.* 205 (2020) 112384.
- [47] N. Aslfattahi, et al., MXene based new class of silicone oil nanofluids for the performance improvement of concentrated photovoltaic thermal collector, *Sol. Energy Mater. Sol. Cell.* 211 (2020) 110526.
- [48] M. Jamshidmofid, M. Bahiraei, Thermohydraulic assessment of a novel hybrid nanofluid containing cobalt oxide-decorated reduced graphene oxide nanocomposite in a microchannel heat sink with sinusoidal cavities and rectangular ribs, *Int. Commun. Heat Mass Tran.* 131 (2022) 105769.
- [49] F.P. Incropera, et al., *Fundamentals of Heat and Mass Transfer* 6, Wiley, New York, 1996.
- [50] H. Maddah, et al., Factorial experimental design for the thermal performance of a double pipe heat exchanger using Al<sub>2</sub>O<sub>3</sub>-TiO<sub>2</sub> hybrid nanofluid, *Int. Commun. Heat Mass Tran.* 97 (2018) 92–102.
- [51] P. Promvongse, S. Skullong, Thermo-hydraulic performance in heat exchanger tube with V-shaped winglet vortex generator, *Appl. Therm. Eng.* 164 (2020) 114424.
- [52] S. Tamna, et al., Heat transfer enhancement in tubular heat exchanger with double V-ribbed twisted-tapes, *Case Stud. Therm. Eng.* 7 (2016) 14–24.

- [53] H. Arjmandi, P. Amiri, M. Saffari Pour, Geometric optimization of a double pipe heat exchanger with combined vortex generator and twisted tape: a CFD and response surface methodology (RSM) study, *Therm. Sci. Eng. Prog.* 18 (2020) 100514.
- [54] P. Promvong, et al., Heat transfer augmentation in a helical-ribbed tube with double twisted tape inserts, *Int. Commun. Heat Mass Tran.* 39 (7) (2012) 953–959.
- [55] S. Bhattacharyya, H. Chattopadhyay, A.C. Benim, Computational investigation of heat transfer enhancement by alternating inclined ribs in tubular heat exchanger, *Prog. Comp. Fluid Dynamics, an Int. J.* 17 (6) (2017) 390–396.
- [56] M.H. Tutar, et al., Convective heat transfer and friction factor characteristics of helical strip inserted annuli at turbulent flow, *Int. J. Heat Mass Tran.* 176 (2021) 121422.
- [57] Y. Xu, M.D. Islam, N. Kharoua, Numerical study of winglets vortex generator effects on thermal performance in a circular pipe, *Int. J. Therm. Sci.* 112 (2017) 304–317.
- [58] R. Faridi Khouzestani, A. Ghafouri, Numerical study on heat transfer and nanofluid flow in pipes fitted with different dimpled spiral center plate, *SN Appl. Sci.* 2 (2) (2020) 298.
- [59] L.S. Sundar, et al., 4-Hydrothermal Properties of Hybrid Nanofluids, in: Z. Said (Ed.), *Hybrid Nanofluids*, Elsevier, 2022, pp. 93–109.
- [60] S.W. Chang, J.Y. Gao, H.L. Shih, Thermal performances of turbulent tubular flows enhanced by ribbed and grooved wire coils, *Int. J. Heat Mass Tran.* 90 (2015) 1109–1124.
- [61] S. Gunes, V. Ozceyhan, O. Buyukalaca, Heat transfer enhancement in a tube with equilateral triangle cross sectioned coiled wire inserts, *Exp. Therm. Fluid Sci.* 34 (6) (2010) 684–691.
- [62] E.-a. Smith, N. Koolnapadol, P. Promvong, Heat transfer behavior in a square duct with Tandem wire coil element insert, *Chin. J. Chem. Eng.* 20 (5) (2012) 863–869.